RSC Advances

ROYAL SOCIETY OF CHEMISTRY

www.rsc.org/advances

Graphic Abstract

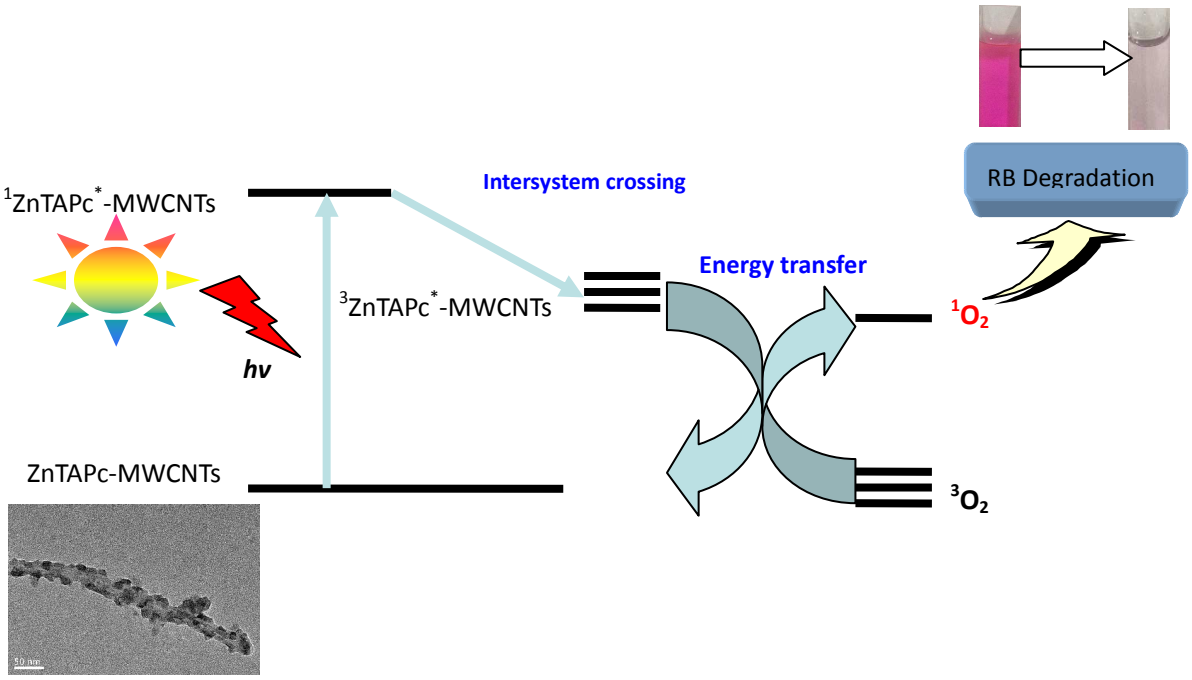

Novel catalyst of zinc tetraamino-phthalocyanine supported by multi-walled carbon nanotubes with enhancement of visible-light photocatalytic activity

Yi Wan [a], Qian Liang [a], Tiantian Cong [a], Xinyu Wang [a], Yuyao Tao [a], Manyou Sun [a], Zhongyu Li [a,b,c]*, Song Xu [a]*

[a] Jiangsu Key Laboratory of Advanced Catalytic Materials and Technology, School of Petrochemical Engineering, Changzhou University, Changzhou 213164, PR China

[b] Key Laboratory of Regional Environment and Ecoremediation (Ministry of Education), Shenyang University, Shenyang 110044, P.R. China

[c]Department of Materials Science and Engineering, Jilin Institute of Chemical Technology, Jilin 132022, PR China

** Corresponding author. Tel.: +86-519-86334771; Fax: +86-519-86334771*

E-mail address: zhongyuli@mail.tsinghua.edu.cn; zhongyuli@cczu.edu.cn; cyanine123@163.com

Abstract: Zinc tetraamino-phthalocyanine (ZnTAPc) supported by multi-walled carbon nanotubes (MWCNTs) hybrid materials were successfully fabricated by the method of chemical grafting and their photocatalysis behavior were reported. The as-products were thoroughly characterized by scanning electron microscopy (SEM), X-ray diffraction (XRD), Raman spectroscopy, transmission electron microscopy (TEM), UV-vis spectra, Thermogravimetric Analysis (TGA) and FT-IR spectra. The results showed that the ZnTAPc nanostructures were not only grown on the multi-walled carbon nanotubes but also uniformly disturbed without aggregation. The photocatalytic studies revealed that the ZnTAPc-MWCNTs hybrid materials exhibited high absorption capacity and excellent simultaneously visible-light-driven photocatalytic performance for rhodamine B (RB) under visible-light irradiation. A possible mechanism for the photodegradation of rhodamine B (RB) was suggested. The hybrid materials provide great potential as active photocatalysts for degrading organic pollutions.

Keywords: Zinc tetraamino-phthalocyanine; Multi-walled carbon nanotubes; Photocatalytic activity; Chemical grafting

1. Introduction

Carbon nanomaterials, including graphene, single-walled carbon (SWCNTs) and multi-walled carbon nanotubes (MWCNTs), because of their unique electronic, mechanism and structural properties, have attracted tremendously scientific attention and wide applications in the past decades [1-10]. MWCNTs are extremely promising as supports for heterogeneous metal catalysts for organic synthesis and fuel cell applications [11-17] due to their good stability, large surface and unique mechanical properties. Some studies have indicated the introduction of MWCNTs can improve the activity and selectivity of these metal

particles, likely due to the large surface areas, the special hollow interiors and excellent electronic properties [18,19]. On the other hand, since the chemical bonding of MWCNTs is solely via sp^2 bonds similar to those of graphite, the high-level electron mobility and electrical conductivity of MWCNTs allow them to use as supports for macrocyclic organic catalysts such as metalloprophyrins and metallophthalocyanines (MPcs).

Phthalocyanines, especially those metal phthalocyanines, could be referred to as attractive alternatives for the visible-light-included photocatalytic decomposition of dye compounds [20-24]. Photoactivity of phthalocyanines arises from their ability to produce the high active $^1O_2$ singlet oxygen species upon photonflux absorption in either UV or visible parts of the spectrum. This singlet oxygen is formed during the extinction mechanism of the excited triplet state, following its collision with molecular O_2. In addition, besides this property, metallophthalocyanines revealed extraordinary molecular stability, negligible toxicity and high thermal stability. The nanoscale particles could enhance the photocatalytic activity and singlet oxygen quantum yields of the phthalocyanines [25, 26]. Zinc phthalocyanine (ZnPc) and its derivatives possess a wide visible light response (600−800 nm) [27]. They can be synthesized with different substituent groups and combined with other compounds by loading or coordination. The synthetic flexibility of phthalocyanines offers great possibilities to modify the length of the connection groups and the positions of substituted groups [28]. Furthermore, zinc phthalocyanine is able to photochemically activate triplet oxygen into singlet oxygen ($^1O_2$), which is frequently used as a non-radical oxidant for oxidizing organic pollutants [29]. However, Metallophthalocyanines are easy to aggregate, leading to markedly decrease the catalytic activity. Therefore, combining the photoresponsive property of both MWCNTs and ZnPc to prepare a photocatalyst with favorable dispersibility and higher photocatalytic activity seems to be extraordinarily vital.

Therefore, we attempted to fabricate a kind of tetraaminophthalocyanine (ZnTAPc) supported by MWCNTs hybrid materials, to solve the problem of aggregation of phthalocyanines and improve its photocatalytic activity. In the present study, the ZnTAPc-MWCNTs hybrid materials were successfully fabricated by the method of chemical grafting and their photocatalysis behaviors were also studied.

2. Experimental

2.1. Synthesis of ZnTAPc

All chemicals were reagent grade and used without further purification. ZnTAPc was synthesized from 3-nitrophthalonitrile, zinc acetate and DBU as described [30]. In a typical experiment, 3-nitrophthalonitrile (0.100 mmol), $Zn(AC)_2{\cdot}2H_2O$ (0.025 mmol), 1-pentanol (30 ml) and DBU (1.5 ml) were put into a three-necked 100 ml round bottom flask. The mixture was then stirred at 130˚C for 8 h. After reaction, the purified ZnTNPc was obtained after washed by 1 mol/L NaOH and then 1 mol/L HCl. Finally, the 1, 8, 15, 22-tetraamino zinc phthalocyanine was obtained after the ZnTNPc reacted with excess Na_2S for 5 h.

2.2. Perparation of ZnTAPc-MWCNTs hybrid materials

The ZnTAPc-MWCNTs hybrid materials were prepared via the method of chemical grafting (Figure 1). The chemical modification of MWCNTs was prepared as follows: MWCNTs were sonicated in a mixture of concentrated sulfuric and nitric acid (3:1 by volume) for 8 h at 80˚C. The obtained carboxyl-terminated MWCNTs (0.05 g) were then refluxed in excess $SOCl_2$ (50 ml) at 70˚C for 24 h. The excess $SOCl_2$ was removed by distillation and the remaining solid was dried in the vacuum. The obtained solid was reacted with ZnTAPc (0.2 g) in 100 ml dimethylformamide (DMF) and mixed with several drops of pyridine at 90˚C for 24

h. The excess ZnTAPc was removed completely by washing with anhydrous redistilled DMSO, leaving a black solid after filtration. The final ZnTAPc-MWCNTs hybrid materials were obtained by drying this solid at ambient temperature.

2.3. Characterization

XRD analyses were carried out with a Rigaku D/Max-2500PC X-ray diffractometer (Rigaku Co.,Japan), using a graphite crystal monochromator to select the Cu-$K_{\alpha 1}$ radiation source at λ = 1.5406 Å, with a step size of 0.02 s^{-1}. Morphologies of the prepared samples were observed on a JSM-6360LA scanning electron microscope (SEM, JEOL, Japan) and a JEM-2100 transmission electron microscope (TEM, JEOL, Japan). Raman spectra were measured at room temperature using a LabRAM XploRA Raman spectrometer (Horiba Jobin Yvon, France) with a 532 nm laser focused on a spot about 3 nm in diameter. UV-vis spectrum was recorded on a UV–vis spectrometer (UV759, Shanghai Precision & Scientific Instrument Co., Ltd., China). Fourier transform infrared spectra (FT-IR) of samples were collected with a Nicolet (PROTéGé 460) spectrometer in the range from 500 to 4000 cm^{-1}. The thermal stability of the materials was carried out using the TG-209-F3 Thermogravimetric Analysis Meter (Nestal Company, Germany).

2.4. Photocatalytic test

The photoreactor was designed with an internal xenon lamp (XHA 1000 W and the average intensity was 28 mW/cm^2) equipped with a cut-off glass filter transmitting > 400 nm surrounded by a water-cooling quartz jacket to cool the lamp, where a 100 mL aliquot of the rhodamine B (RB) solution with an initial concentration of 25 mg/L in the presence of ZnTAPc-MWCNTs hybrid catalysts (50 mg). The volume of initial RB solution is 50 ml. The

solution was stirred in the dark for 30 min to obtain a good dispersion and established adsorption-desorption equilibrium between the organic molecules and the catalyst surface. Decreases in the concentrates of dyes were analyzed by a UV–vis spectrometer (UV759, Shanghai Precision & Scientific Instrument Co., Ltd., China). At given intervals of illumination, the samples of the reaction solution were taken out and analyzed. The photodegradation of methyl orange (MO), was also carried out by the similar procedure.

3. Results and discussion

The FT-IR spectra of oxidized-MWCNTs (c), ZnTAPc (b) and ZnTAPc-MWCNTs (a) are shown in Figure 2. For ZnTAPc, the bands at 1341, 1109, 1028, 738 cm^{-1} are assignable to the skeleton stretching of ZnTAPc. Carboxylic acid-functionalized MWCNTs showed two strong absorption bands at 3440 and 1715 cm^{-1}, associating with O-H stretching and C=O stretching in carboxyl, respectively. Another strong band at 1226 cm^{-1} was assigned to the C–O stretching in carboxylic. For ZnTAPc-MWCNTs, the peaks appeared in ZnTAPc can be found in ZnTAPc-MWCNTs, but are not present in oxidized MWCNTs. The peaks at 1721 and 1530 cm^{-1} were assigned to amide and the amide linkages between ZnTAPc and MWCNTs. In addition, two broad peaks around 3452 and 3337 cm^{-1}, corresponded with the dissociation of N–H stretching band from ZnTAPc, disappeared in the spectra of ZnTAPc-MWCNTs. All these observations indicated that ZnTAPc had been attached onto MWCNTs successfully.

Figure 3 shows the TEM images of oxidized-MWCNTs (a), ZnTAPc-MWCNTs (b), pure ZnTAPc (c), and HRTEM image of ZnTAPc-MWCNTs (d). Compared with oxidized-MWCNTs, the interfacial area of the ZnTAPc-MWCNTs was found to be rough due to the formation of a whiskered ZnTAPc (Figures 3b and 3d). The TEM images of the

ZnTAPc-MWCNTs exhibited a roughened and shortened feature with ZnTAPc uniformly assembling in the convex surfaces of MWCNTs. The interfacial area of the ZnTAPc-MWCNTs was found to be rough due to the formation of a whiskered ZnTAPc (Figure 3d). From these figures, we can observe the coverage of phthalocyanines on the sidewall of MWCNTs. The ZnTAPc-MWCNTs appears to be made of bundles composed of tubes with specific rugged surface and a layer of about 2-5 nm in thickness immobilized onto the sidewall of MWCNTs. Moreover, the integrity of tubular individual nanohorns before and after coating ZnTAPc is also noticeable in the magnified images, indicating that the surface functionalization with ZnTAPc via covalent π-π stacking produces insignificant damage to the intrinsic structures of MWCNTs. The resulting hybrid materials exhibited a stretched and shortened feature with phthalocyanines uniformly assembling on the convex surface of MWCNTs (Figure 3b). However, ZnTAPc exhibited poor dispersibility with clusters congregated while the density of ZnTAPc on the MWCNTs was improved (Figure 3c).

Compared with the oxidized-MWCNTs (Figure 4a), the SEM image of ZnTAPc-MWCNTs hybrid materials show an appreciable increase in thickness (Figure 4b), confirming the formation of nanohybrids, probably due to the amide linkages between ZnTAPc and MWCNTs. After immobilized on MWCNTs, nanoparticles of phthalocyanines with a diameter from several to tens of nanometers are clearly observed on MWCNTs walls. Compared with the SEM image of pure ZnTAPc (Figure 4c), ZnTAPc dots are dispersed in each threadlike MWCNT matrix (Figure 4b), showing good dispersibility with MWCNT materials.

The X-ray diffraction (XRD) patterns of oxidized-MWCNTs, ZnTAPc and

ZnTAPc-MWCNTs are shown in Figure 5. Compared with the curve b in Figure 5, the diffraction peaks of the ZnTAPc-MWCNTs (the curve c) were broad and weak, indicating a small crystal size or poor crystallinity of ZnTAPc in the ZnTAPc-MWCNTs hybrid materials. Moreover, the characteristic peaks of the ZnTAPc-MWCNTs became weak because the ZnTAPc was well dispersed on the surface of MWCNTs. All of the reflection peaks of ZnTAPc-MWCNTs could be indexed as ZnTAPc, indicating the ZnTAPc nanostructures were successfully fabricated on the surface of MWCNTs.

We evaluated UV-vis spectra of free ZnTAPc and ZnTAPc-MWCNTs in DMF solution (Figure 6). Free ZnTAPc shows two distinguishable adsorption bands, peaked at 681 and 764 nm, corresponding to the presence of a dimer and monomer of ZnTAPc, respectively. Upon complexation of MWCNTs, the absorption band of the dimer and the monomer peak turned to broader and weaker, accompanying a blue shift to 678 and 761 nm, respectively. The phenomena indicated that a strong π-π interaction between MWCNTs and ZnTAPc, resulted in the deaggregation of ZnTAPc.

Covalent attachment of ZnTAPc to MWCNTs support was further confirmed by Raman spectroscopy. The Raman spectra of ZnTAPc-MWCNTs and MWCNTs are shown in Figure 7. The oxidized-MWCNTs displayed a G mode at 1576 cm^{-1} accompanied by a strong tangential peak at 1347 cm^{-1}, corresponding to the D mode due to sp^3-hybridized carbons. The grafting of ZnTAPc of the oxidized-MWCNTs resulted in a substantial decrease in the number of sp^3-hybridized carbons with a concomitant decrease in the D mode and a increase in the tangential G mode associated with sp^2-hybridized carbons from the nanotube sidewalls. This decrease in the ratio of the sp^3:sp^2 ratio is described by the D:G ratio, suggesting that the

continuous delocalization of electrons throughout the nanotubes has been highly disrupted due to covalent attachment of the ZnTAPc to the nanotubes. Thus, the conjugates of tetra-amino substituted phthalocyanines with MWCNTs were synthesized.

The amounts of ZnTAPc covalently linked with the MWCNTs were determined by TGA. Figure 8 shows the TGA measurements for pure MWCNTs and ZnTAPc-MWCNTs hybrid materials. This figure shows the percent mass loss as a function of temperature at 10°C/min heating rate under a nitrogen atmosphere. As shown in Figure 8, the ZnTAPc segments in ZnTAPc-MWCNT hybrid materials can be completely degraded without any inert residue remaining at 800˚C. It is clear seen that there is about 39.9% of ZnTAPc-MWCNTs hybrid materials present at 800˚C. In contrast, there is 94.9% of pure MWCNTs present at this temperature. By definitely value the weights of pure MWCNTs and ZnTAPc-MWCNTs hybrid materials after thermal degradation at 800˚C, the amount of ZnTAPc bonded to MWCNTs is calculated to be 55% by weight. Combining with the mentioned FT-IR and TEM measurements, it is believed that MWCNTs covalently bonded by zinc tetraamino-phthalocyanines are indeed obtained.

To test the photocatalytic activity of ZnTAPc-MWCNTs hybrid materials for the degradation of organic pollutions, rhodamine B (RB) was selected as a representative dye pollutant of industrial wastewaters. The photocatalytic activities of the ZnTAPc-MWCNTs hybrid materials were evaluated by the degradation of RB in aqueous solution under visible-light irradiation. Before studying and comparing the activities of the ZnTAPc-MWCNTs hybrid materials, the bleaching of RB in the absence of any catalysts was first examined. As shown in Figure 9a, RB degradation without any photocatalyst was

performed, and the results illustrated that the degradation of RB was very slow in the absence of photocatalyst under visible-light irradiation, only 2% of RB was degraded under the irradiation with visible light. Next, the photocatalytic activities of MWCNTs were investigated. It can be clearly seen that the MWCNTs had almost no photocatalytic activity under the visible-light irradiation, expect decent adsorption for RB (18.5%), which could attributed to the high specific surface area of the carbon nanotubes. Irradiation of aqueous solutions of RB (25 mg/L) after the ZnTAPc immobilized onto MWCNTs led to an obvious decrease of RB concentration. The excellent photoactivity depended on the structure of the immobilized phthalocyanines, implying that the degradation of RB was initiated by its reaction with the reactive oxygen species produced upon exciting the phthalocyanines with the appropriate wavelength of light. It seems very important to consider whether photocatalysis could still happen effectively after the adsorption of RB to ZnTAPc-MWCNTs hybrid materials reached equilibrium. In the presence of ZnTAPc-MWCNTs hybrid materials but in the darkness, the removal rate of RB was 37.9% within 30 min. It was found that almost no change occurred during the next 240 min, which was attributed to the good adsorption of ZnTAPc-MWCNTs, while the adsorption of RB was close to saturation by the end of the initial 30 min. Indeed, at same conditions, 88.0% of the RB was degraded under the irradiation with visible light. On the other hand, pure ZnTAPc barely showed activity for RB photodegradation (54.3%) due to the aggregation of ZnTAPc decreased the photoactivity, while ZnTAPc-MWCNTs demonstrates good photocatalytic activity with a degradation rate of 0.5144 h^{-1} (Figure 9b). The degradation efficiency of the as-prepared samples was defined as C_0/C, and the rate was estimated based on

$$\ln (C_0/C) = kt$$

Where C_0 is the equilibrium concentration of RB after 30 min dark adsorption, C is the RB concentration remaining in the solution at irradiation time (h), and k is the observed rate constant. The introduction of MWCNTs promoted the degradation of RB effectively. The k value was 0.5144 h^{-1}, which was 6.8 and 11.4 times higher than that of pure ZnTAPc (0.0659 h^{-1}) and MWCNTs (0.0415 h^{-1}), respectively. Obviously, the coupling of ZnTAPc and MWCNTs via the covalent attachment created an excellent hybrid photocatalyst. The enhanced photoactivity may be ascribed to the improvement in charge transmission between the MWCNTs and ZnTAPc prolonged the lifetime of charge carriers. Moreover, the photoactivity of the hybrid photocatalyst was also affected by the surface contact between particles. The ZnTAPc-MWCNTs hybrid materials had higher contact interfaces between ZnTAPc and MWCNTs, resulting in higher photocatalytic efficiency. Table 1 shows the photocatalytic activity of as-prepared of ZnTAPc-MWCNTs hybrid photocatalyst by comparison of the metallophthalocyanine and other metal photocatalysts. It was found that 88.0% of the RB was degraded under the visible light irradiation with ZnTAPc-MWCNTs as photocatalyst, confirming the as-prepared ZnTAPc-MWCNTs hybrid materials showed good photocatalytic performance.

Figure 10 shows the photocatalytic activities of RB and MO in the presence of ZnTAPc-MWCNTs hybrid photocatalyst. It can be seen that the RB and MO dyes are photodegraded efficiently over the ZnTAPc-MWCNTs photocatalysts, 85.6% of the MO solution was degraded after irradiation for 4 h, The photocatalytic results indicated that the as-prepared ZnTAPc-MWCNTs hybrid materials are excellent photocatalyst for the

photodegradation of RB and MO. The introduction of MWCNTs could greatly promote the photocatalytic activity of ZnTAPc due to the MWCNTs as catalyst support prevented the aggregation of ZnTAPc and increased the catalytic active sites. Moreover, the stability of the ZnTAPc-MWCNTs hybrid photocatalysts was examined for degradation of RB during a three cycle experiment, which was very important for the ZnTAPc-MWCNTs hybrid photocatalyst to apply in environmental problems. As shown in Figure 11, each experiment was carried out under identical conditionals, and after a three- cycle experiment, the photocatalytic activity of RB remained almost unchanged. The high photocatalytic performance of ZnTAPc-MWCNTs was effectively maintained except for 3.7 % decrease in photocatalytic efficiency. It was indicated that the ZnTAPc-MWCNTs hybrid photocatalysts displayed an efficient photoactivity for the degradation of organic pollutions under visible light irradiation and could be easily be separated for reuse.

Mechanism of photodegradation of organic pollutions in presence of oxygen and porphyrin or phthalocyanines, either immobilized or in solution [31-32] or in solution [33-34], may involve both type I (electron or atom transfer) and/or type II (singlet oxygen) processes. To test whether the mechanism of reactions of the systems in these studies involves electron transfer and/or singlet oxygen, photodegradation reactions were carried out in the presence and absence of oxygen.

The photodegradation of RB catalyzed by ZnTAPc-MWCNTs hybrid materials was performed in air and in a solution of beta-carotene ($C_{40}H_{56}$, $^1O_2$ scavenger). As shown in Figure 12, the photodegradation of RB was virtually complete after 4 h irradiation when experiment was carried out in air solutions, while under oxygen-free conditions only 4.8%

conversion was achieved. The addition of beta-carotene greatly decreased the photocatalytic activity of ZnTAPc-MWCNTs, indicating that $^1O_2$ is the dominant active species [35]. Introduction of singlet oxygen scavenger halted the reaction strongly suggesting that single oxygen is involved in the mechanism of photodegradation (type II mechanism).

In heterogeneous reaction for ZnTAPc-MWCNTs under visible light irradiation, the generation of singlet oxygen is an adopted photocatalytic mechanism [36]. On the basis of the above results and the earlier reports on the photocatalytic oxidation of pollutants, a proposed mechanism of visible light-induced photodegradation of RB with the ZnTAPc-MWCNTs hybrid materials is elucidated as follows:

$$\text{ZnTAPc - MWCNTs} \xrightarrow{hv} {}^1\text{ZnTAPc}^* \text{- MWCNTs} \quad (1)$$

$${}^1\text{ZnTAPc}^* \text{- MWCNTs} \xrightarrow{ISC} {}^3\text{ZnTAPc}^* \text{- MWCNTs} \quad (2)$$

$${}^3O_2 + {}^3\text{ZnTAPc}^* \text{- MWCNTs} \longrightarrow \text{ZnTAPc - MWCNTs} + {}^1O_2 \quad (3)$$

$${}^1O_2 + \text{RB} \longrightarrow \text{Oxidtaion product} \quad (4)$$

The ZnTAPc-MWCNTs was excited by visible light irradiation to form the single line excitation state (^{1}ZnTAPc*-MWCNTs) (Eq. (1)), and then ^{1}ZnTAPc*-MWCNTs can turn into the excited triplet states sensitizer of ^{3}ZnTAPc*-MWCNTs (Eq. (2)) by irradiation and inersystem crossing (ISC). ^{3}ZnTAPc*-MWCNTs can interact with the ground state triplet oxygen ($^3O_2$) to generate the highly active singlet oxygen ($^1O_2$) (Eq. (3)), resulting in the decomposition of RB (Eq. (4)).

4. Conclusions

In summary, by using a chemical grafting process, the ZnTAPc-MWCNTs hybrid

materials were successfully fabricated. Furthermore, the ZnTAPc-MWCNTs exhibited not only high absorption capacity, but also excellent photocatalytic activities for RB under visible light. The prepared ZnTAPc-MWCNTs powders displayed much higher photocatalytic activity than single ZnTAPc or MWCNTs under visible light irradiation. A possible mechanism for "singlet oxygen process" was suggested. Also, it is expected that the ZnTAPc-MWCNTs hybrid materials with high photoactivity will greatly promote their industrial application to eliminate the organic pollutions from wastewater. Moreover, this research offers a new strategy to design high efficient MWCNTs-supported catalysts by utilizing the special sp^2-hybridized surface of MWCNTs for various applications in organic synthesis, green chemistry and environmental treatment.

Acknowlwdgements

This work was financially supported by Open Fund of Key Laboratory of Regional Environment and Eco-remediation of Ministry of Education, China (SYU-KF-E-12), Open Fund of Key Laboratory of Contaminated Environment Control and Regional Ecology Safety, Shenyang University, China (SYU-KF-L-12), Project Funded by the Priority Academic Program Development of Jiangsu Higher Education Institutions, Project for Six Major Talent Peaks of Jiangsu Province (2011-XCL-004) and Natural Science Foundation of Changzhou City, China (CJ20140053).

References:

[1] C. Chung, Y. K. Kim, D. Shin, S. R. Ryoo, B. H. Hong and D. H. Min, Acc. Chem. Res., 2013, 46, 2211-2224.

[2] G. Qin, J. Zhang and C. Wang, J. Alloys Compd., 2015, 635, 158-162.

[3] M. F. De Volder, S. H. Tawfick, R. H. Baughman and A. J. Hart, Science, 2013, 339, 535-539.

[4] Y. Song, K. Qu, C. Zhao, J. Ren and X. Qu, Adv. Mater., 2010, 22, 2206-2210.

[5] M. Calvaresi, F. Zerbetto, Acc. Chem. Res., 2013, 46, 2454-2463.

[6] G. Peng, L. Zhang, X. Yang, S. Duan, G. Liang and Y. Huang, J. Alloys Compd., 2013, 570, 1-6.

[7] Z. Liu, A. C. Fan, K. Rakhra, S. Sherlock, A. Goodwin, X. Chen, Q. Yang, D. W. Felsher and H. Dai, Angew. Chem. Int. Ed., 2009, 48, 7668-7672.

[8] N. S. Andryushina, O. L. Stroyuk, Appl. Catal. B, 2014, 148, 543-549.

[9] Q. Cheng, M. Wu, M. Li, L. Jiang and Z. Tang, Angew. Chem. Int. Ed., 2013, 13, 3838-3843.

[10] T. N. Lambert, C. A. Chavez, B. Hernandez-Sanchez, P. Lu, N. S. Bell, A. Ambrosini, T. Friedman, T. J. Boyle, D. R. Wheeler and D. L. Huber, J. Phys. Chem. C., 2009, 113, 19812-19823.

[11] B. Yoon, C. M. Wai, J. Am. Chem. Soc., 2005, 127, 17174-17175.

[12] A. Solhy, B. F. Machado, J. Beausoleil, Y. Kihn, F. Goncalves, M. F. R. Pereira, J. J. M. Orfao, J. J. Figueiredo, J. L. Faria and P. Serp, Carbon, 2008, 46, 1194-1207.

[13] S. Wang, X. Shi, G. Shao, X. Duan, H. Yang and T. Wang, J. Phys. Chem. Solids, 2008, 69, 2396-2400.

[14] B. Liu, Z. Y. Li, S. Xu, D. Han and D. Lu, Mater. Lett., 2014, 131, 229-232.

[15] H. Vu, F. Goncalves, R. Philippe, E. Lamouroux, M. Corrias, Y. Kihn, D. Plee, P. Kalck

and P. Serp, J. Catal., 2006, 240, 18-22.

[16] J. Q. Wei, J. Ding, X. F. Zhang, D. H. Wu, Z. C. Wang, J. B. Luo and K. L. Wang, Mater. Lett., 2005, 59, 322-325.

[17] J. Li, Y. B. Wang, J. D. Qiu, D. C. Sun and X. H. Xia, Anal. Bioanal. Chem., 2005, 383, 918-922.

[18] H. B. Zhang, X. Dong, G. D. Lin, X. L. Liang and H. Y. Li, Chem. Commun., 2005, 40, 5094–5096.

[19] X. Pan, Z. Fan, W. Chen, Y. Ding, H. Luo and X. Bao, Nat. Mater., 2007, 6, 507-511.

[20] M. Y. Zhang, C. L. Shao, Z. C. Guo, Z. Y. Zhang, J. B. Mu, P. Zhang and T. P. Cao, Appl. Mater. Interfaces, 2011, 3, 2573-2578.

[21] E. Marais, R. Klein, E. Antunes and T. J. Nyokong, Mol. Catal. A: Chem., 2007, 261, 36-42.

[22] G. Palmisano, M. C. Gutierrez, M. L. Ferrer, M. D. Gil-Luna, V. Augugliaro, S. Yurdakal and M. Pagliaro, J. Phys. Chem. C., 2008, 112, 2667-2670.

[23] H. J. Mackintosh, P. M. Budd and N. B. McKeown, J. Mater. Chem., 2008, 18, 573-578.

[24] S. Makhseed, F. Al-Kharafi, J. Samuel and B. Ateya, Catal. Commun., 2009, 10, 1284-1287.

[25] M. E. Wieder, D. C. Hone, M. J. Cook, M. M. Handsley, J. Gavrilovic and D. A. Russell, J. Photochem. Photobiol. Sci., 2006, 5, 727-734.

[26] S. FitzGerald, A. Beeby, I. Chambrier, M. J. Cook and D. A. Russell, Langmuir, 2002, 18, 2985-2987.

[27] Y. Wan, Q. Liang, Z. Y. Li, S. Xu, X. J. Hu, Q. L. Liu and D. Y. Lu, Mol. Catal. A: Chem.,

2015, 402, 29-36.

[28] C. Zhou, Y. Liu, X. Zhao, Inorg. Chim. Acta., 2015, 425, 11–16.

[29] M. Gao, N. Li, W. Lu, W. Chen, Appl. Catal. B: Environ., 2014, 147, 805–812.

[30] B. N. Achar, G. M. Fohlen, J. A. Parker and Keshavayya, Polyhedron, 1987, 6, 1463-1467.

[31] M. Silva, M. E. Azenha, M. M. Pereira, H. D. Burrows, M. Sarakha, C. Forano, M. F. Ribeiro and A. Fernandes, Appl. Catal. B, 2010, 100, 1-9.

[32] M. A. Zanjanchi, A. Ebrahimian and M. Arvand, J. Hazard Mater., 2010, 175, 992-1000.

[33] X. F. Zhang, X. Li and L. J. Niu, J. Fluoresc., 2009, 19, 947-954.

[34] C. Yang, L. Ye, L. Tian, T. Peng, K. Deng and L. Zan, J. Colloid Inter. Sci., 2011, 253, 533-541.

[35] C. J. P. Monteiro, M. M. Pereira, M. E. Azenha and H. D. Burrows, Photochem. Photobiol. Sci., 2005, 4, 617-624.

[36] X. F. Zhang, X. Li, L. J. Niu, L. Sun and L. Liu, J. Fluoresc., 2009, 19, 947-954.

[37] Z. C. Guo, J. B. Mu and B. Chen, Ceram. Int., 2015, 41, 4916-4922.

[38] L. X. Zhang, J. Zhang, H. F. Jiu, C. H. Ni, X. Zhang and M. L. Xu, J. Phys. Chem. Solids, 2015, 86, 82-89.

[39] M. Fereshteh, R. M. Mohammad, S. Faezeh and S. N. Masoud, RSC Adv., 2014, 4, 27654-27660.

[40] Z. C. Guo, C. L. Shao, J. B. Mu, M. Y. Zhang, Z. Y. Zhang, Z. Peng, B. Chen and Y. C. Liu, Catal. Commun., 2011, 12, 880-885.

[41] Y. R. Su, C. H. Ding, Y. L. Yuan, H. Wang, L. Q. Ye, X. L. Jin, H.Q. Xie and C. Liu, Appl.

Surf. Sci., 2015, 346, 311-316.

Table 1. Photocatalytic activities toward the degradation of RB of some reported catalysts.

Catalyst	Reaction time, min	Removal percentage, %	Concentration of RB, g/L	Ref.
CuTNPc/TiO_2	240	87	10	20
FeTNPc	300	90	10	37
TiO_2/RGO	210	75	10	38
NiO	180	80	10	39
CdPc/PAN	420	85	10	40
Bi_5O_7Br	120	85	11	41
ZnTAPc-MWCNTs	240	88	25	This work

Figures captions

Fig. 1. Illustration of preparation process of ZnTAPc-MWCNTs hybrid materials.

Fig. 2. FT-IR spectra of oxidized ZnPc-MWCNTs (a), ZnPc (b) and MWCNTs (c).

Fig. 3. TEM images of oxidized-MWCNTs (a), ZnTAPc-MWCNTs (b), pure ZnTAPc (c), and HRTEM image of ZnTAPc-MWCNTs (d).

Fig. 4. SEM images of oxidized-MWCNTs (a), ZnTAPc-MWCNTs (b) and pure ZnTAPc (c).

Fig. 5. XRD spectra of oxidized MWCNTs (a), ZnTAPc (b) and ZnTAPc-MWCNTs (c).

Fig. 6. UV-vis spectra of ZnTAPc and ZnTAPc-MWCNTs hybrid materials in DMF. Inset shows a photograph of ZnTAPc-MWCNTs (left) and ZnTAPc dispersed in DMF.

Fig. 7. Raman spectra of ZnTAPc-MWCNTs (a) and MWCNTs (b).

Fig. 8. TGA curves of pure MWCNTs and ZnTAPc-MWCNTs hybrid materials.

Fig. 9. Absorption and photocatalytic of RB by different photocatalysts with the same weight under visible-light irradiation (a), kinetic plot for ZnTAPc-MWCNTs, ZnTAPc and MWCNTs in photooxidation of RB (b).

Fig. 10. Photodegradation of different organics over 50 mg ZnTAPc-MWCNTs.

Fig. 11. Photocatalytic degradation of RB over ZnTAPc-MWCNTs under visible-light irradiation for 3 cycles.

Fig. 12. Photodegradation rate of RB in the presence of beta-carotene at different periods of time.

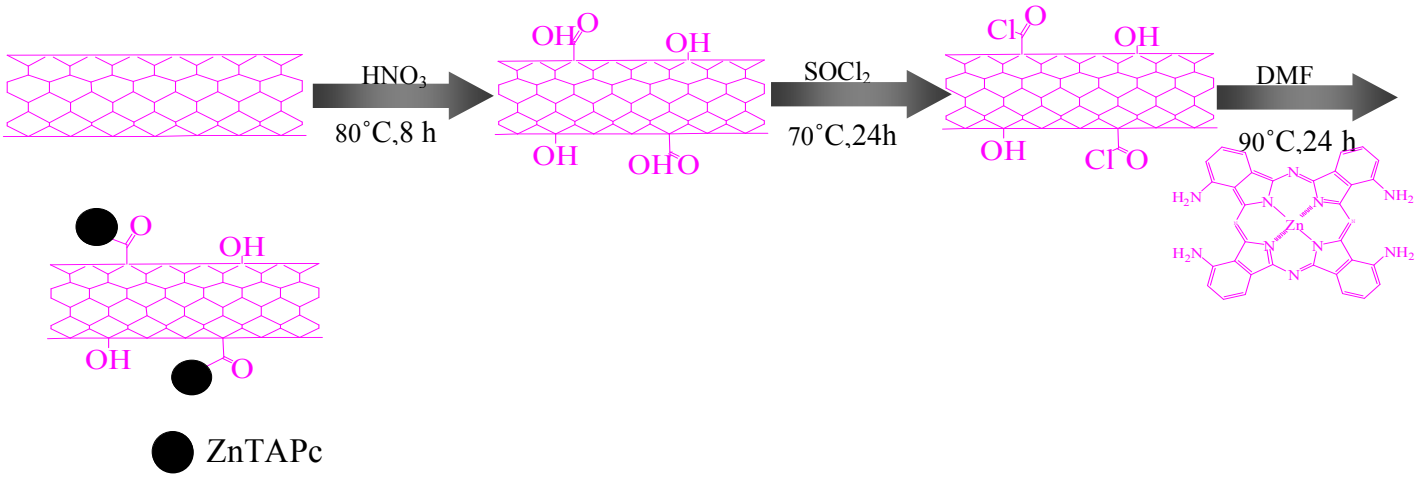

Figure 1

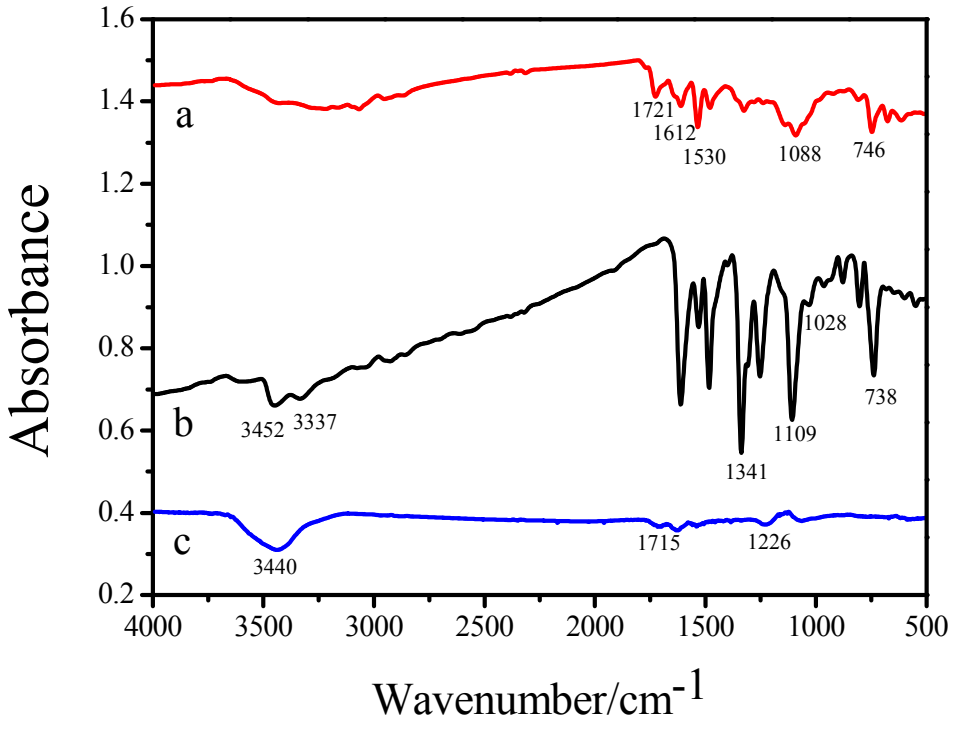

Figure 2

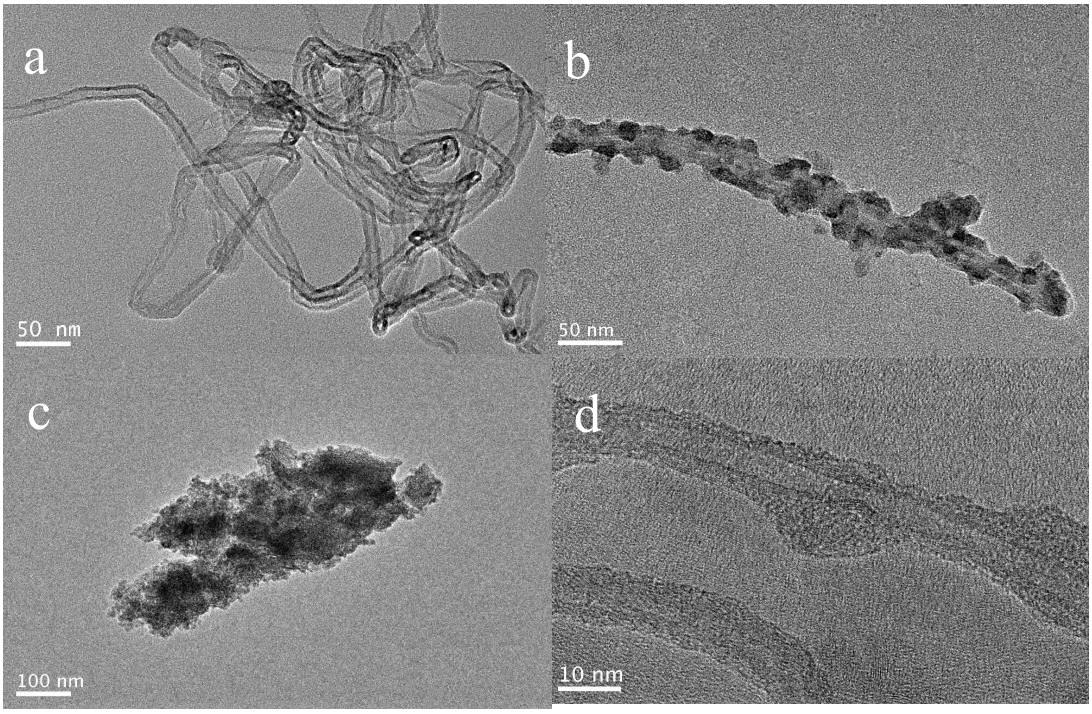

Figure 3

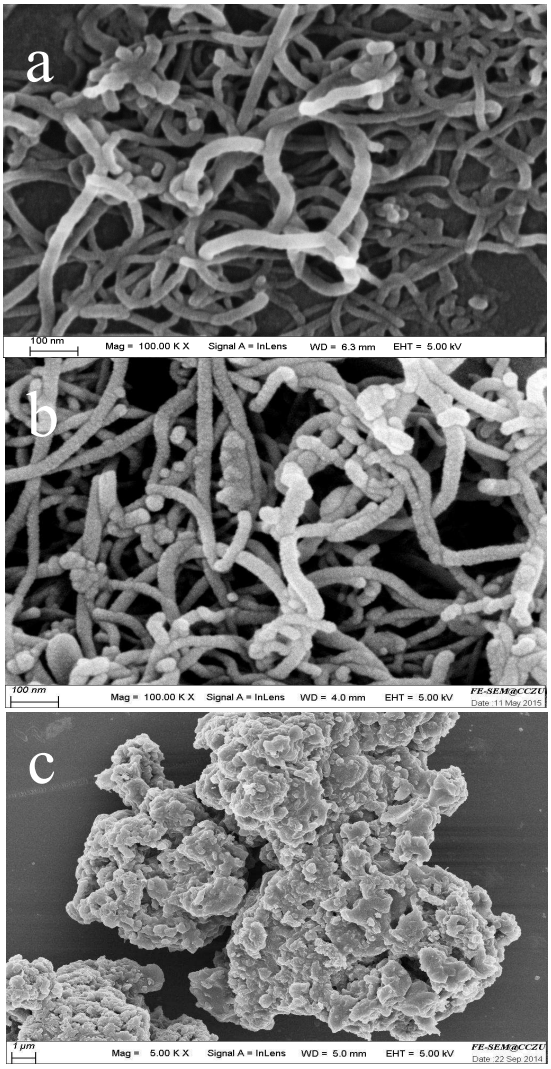

\

Figure 4

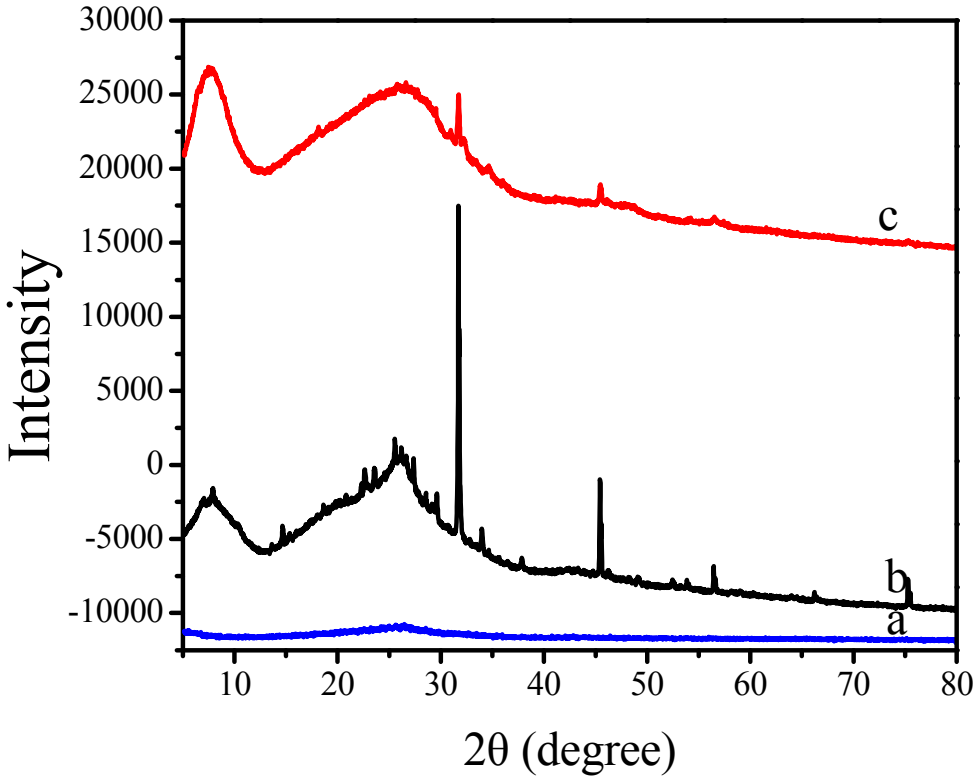

Figure 5

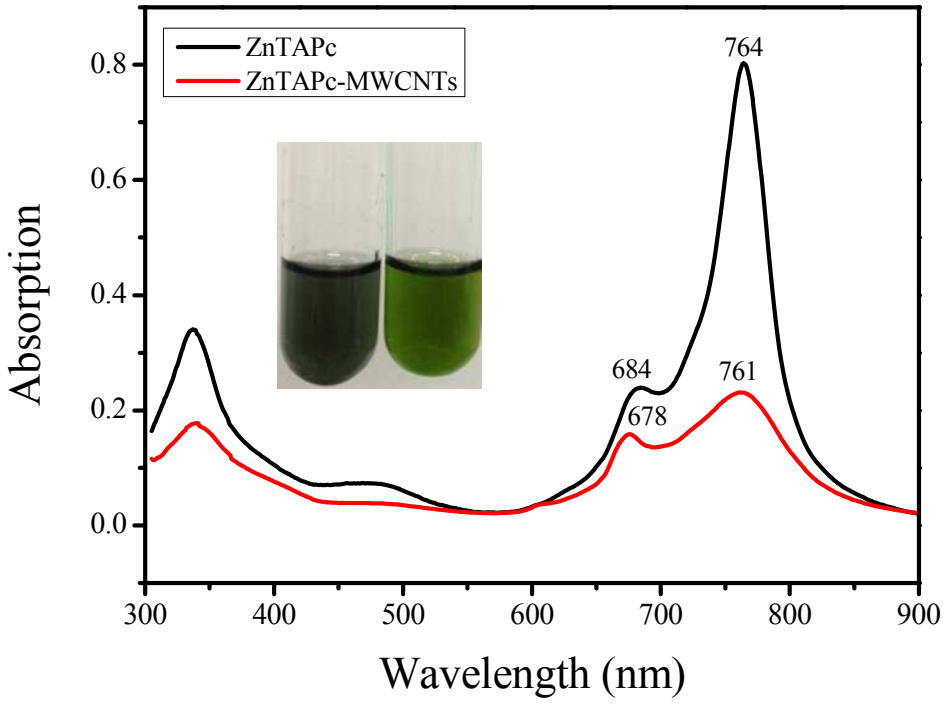

Figure 6

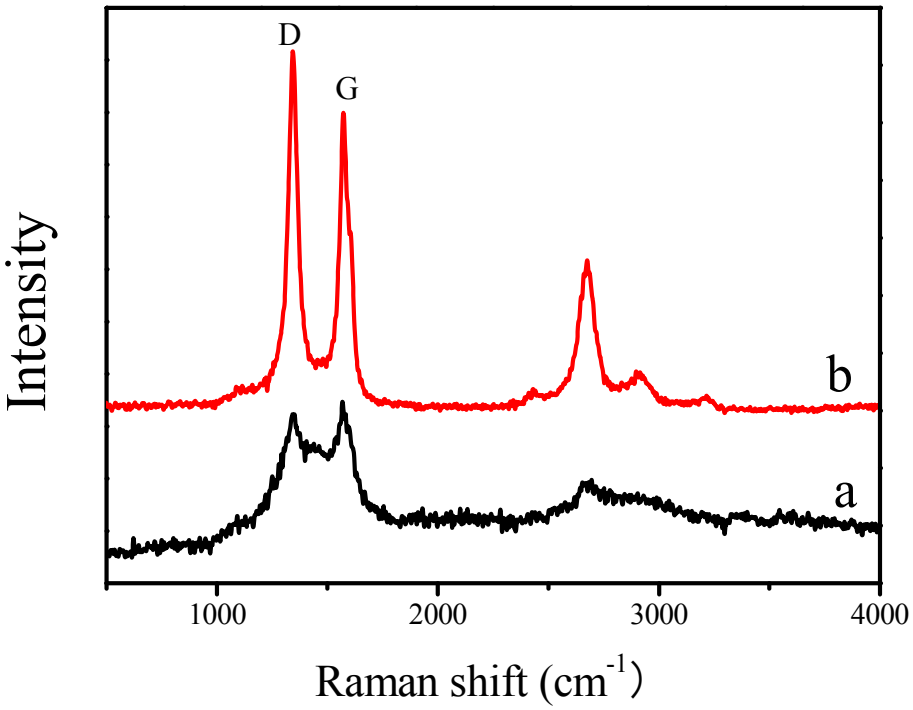

Figure 7

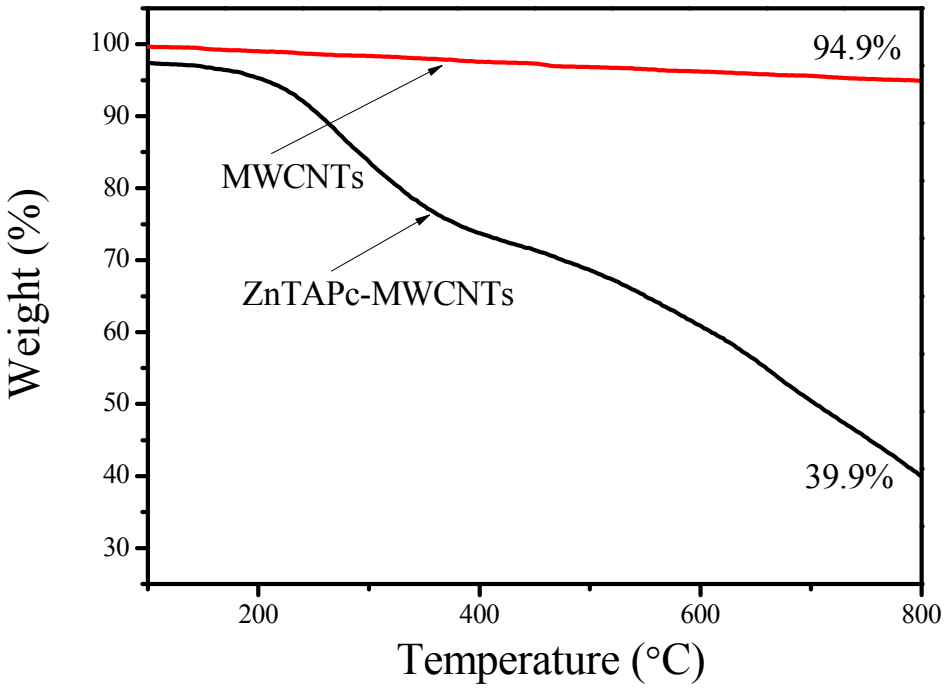

Figure 8

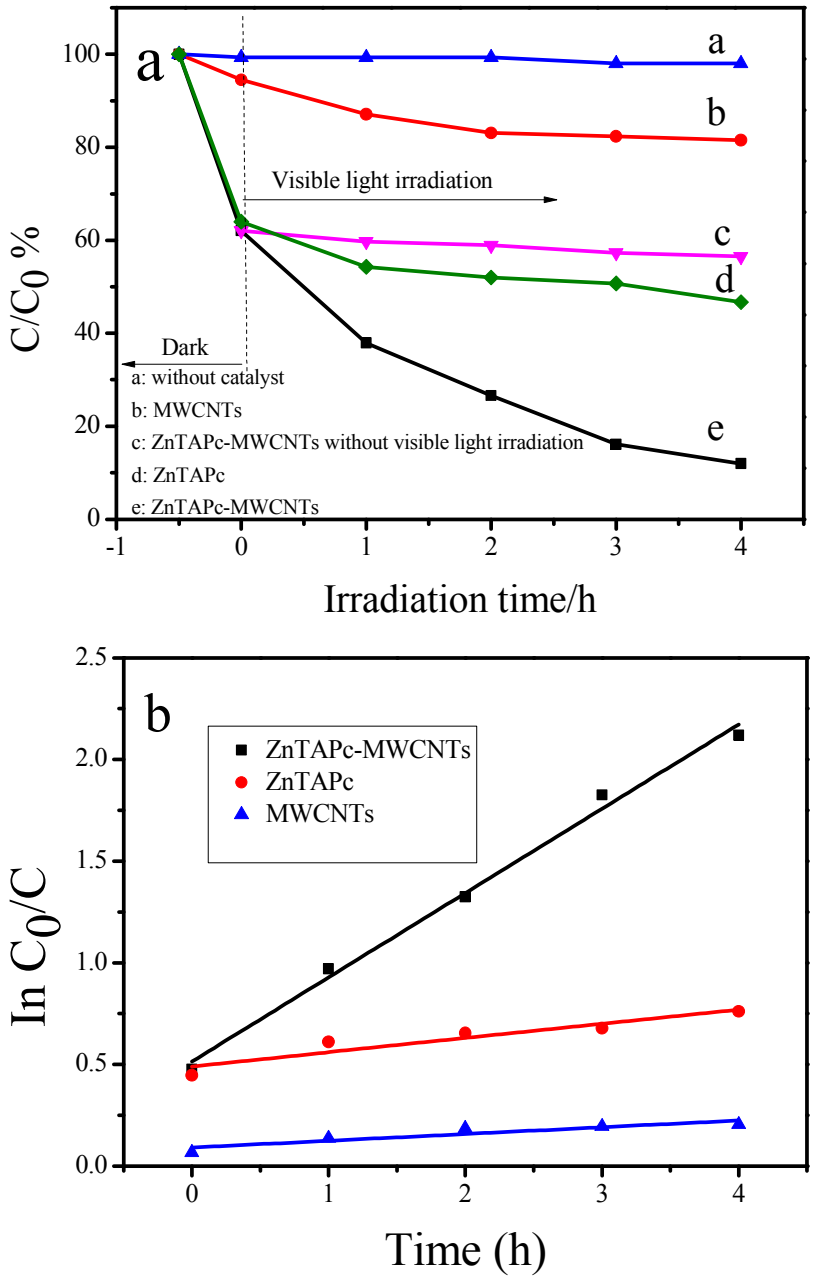

Figure 9

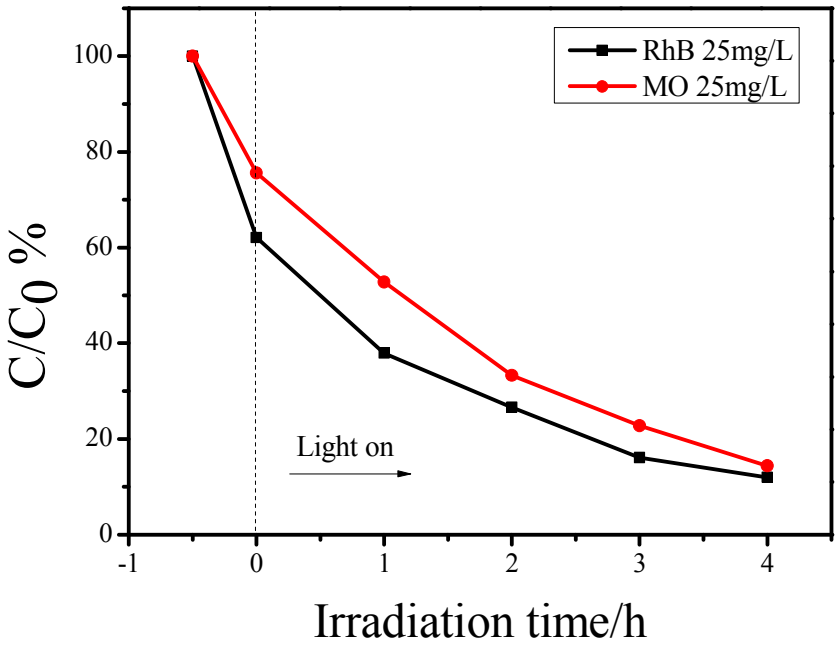

Figure 10

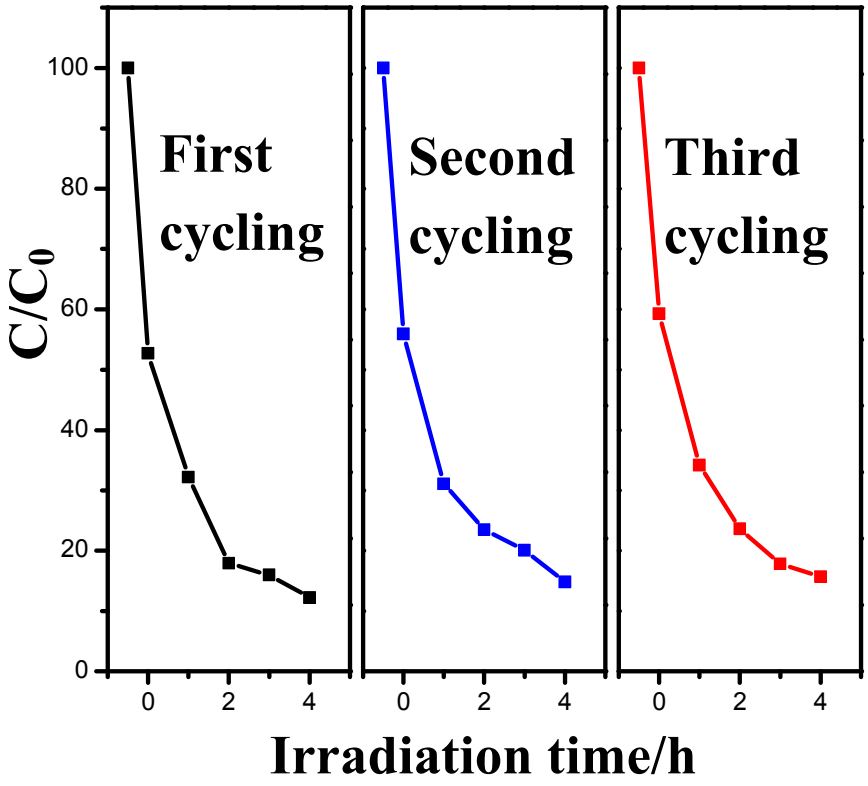

Figure 11

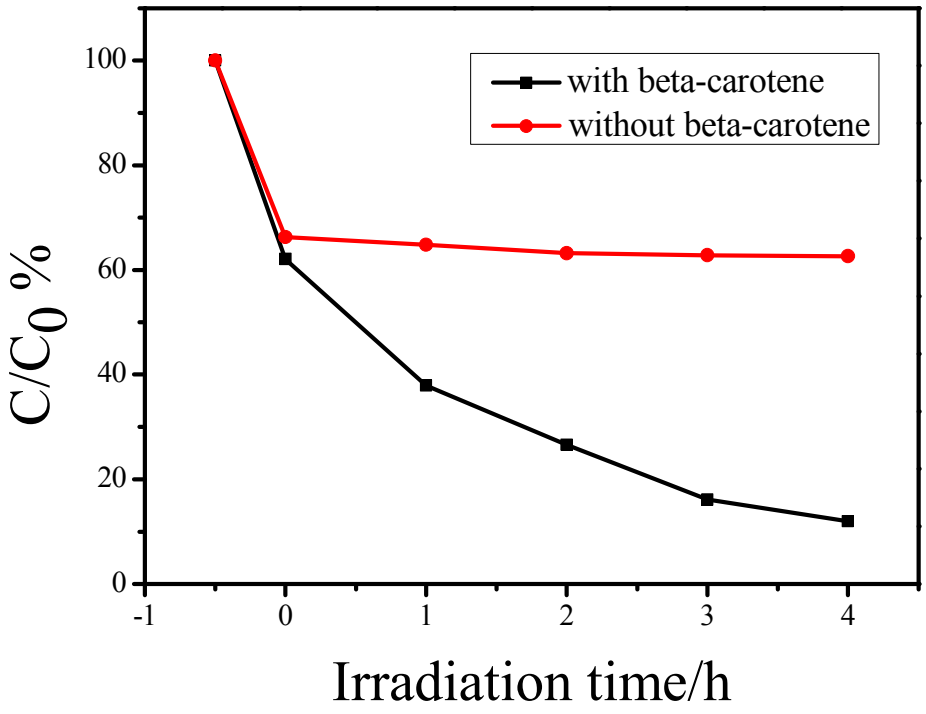

Figure 12